Received 14 July 2025; Accepted 29 September 2025
https://doi.org/10.48612/letters/2025-4-263-269
https://elibrary.ru/ldnbzq

Patterns of formation of micro-arc calcium phosphate coatings on different types of metal substrates

A. V. Ugodchikova[1], M. B. Sedelnikova[†2], T. V. Tolkacheva[2], P. V. Uvarkin[2], M. A. Khimich[2], Yu. P. Sharkeev[2], A. D. Kashin[2], I. A. Glukhov[2]

[†]smasha5@yandex.ru

[1]Research Institute of Technical Physics and Automation, Moscow 115230, Russia
[2]Institute of Strength Physics and Materials Science, Siberian Branch of the Russian Academy of Sciences, Tomsk 634055, Russia

Abstract: The development of novel materials for traumatology and orthopedics is the major focus of current research in the field of medical materials science. Bioinert titanium alloys continue to be widely used for the production of medical implants, while new-generation materials based on bioresorbable magnesium alloys are also gaining popularity. A promising method for modifying the surface of these implants is through the formation of biocoatings using the micro-arc oxidation (MAO) technique. Comparative studies of the formation patterns of micro-arc calcium phosphate (CaP) coatings on the surface of titanium VT1-0, Ti-40 wt.% Nb and magnesium Mg-0.8 wt.% Ca alloys were carried out in this work. The morphology of the coatings, their microstructure, and phase composition were studied by scanning electron microscopy (SEM), transmission electron microscopy (TEM), and powder X-ray diffraction (XRD) methods. It is established that the MAO process on magnesium substrates is characterized by the highest value of the initial current density, equal to 0.68 A/cm^2. The thickness of the non-porous transition oxide layer of MgO is almost 10 times higher than the thickness of oxide layers for coatings on titanium alloys. CaP coatings deposited on magnesium substrates have the highest values of thickness, roughness and adhesion strength, equal to 118 μm, 8.8 μm, and 19.2 N, respectively. The reasons for the differences in the MAO processes implemented on titanium and magnesium alloys, as well as in the properties of the resulting coatings, are the different types of conductivity and the different electrophysical properties of titanium, niobium, and magnesium oxides that make up the transition oxide layer between the coating and the substrate.

Keywords: micro-arc oxidation, oxide layer, porous structure, band gap, relative permittivity

Acknowledgements: *The work was performed according to the Government research assignment for ISPMS SB RAS, project FWRW-2021-0007.*

1. Introduction

Metals are the preferred materials for orthopedic and surgical implants due to their superior mechanical properties [1]. Currently, titanium and its alloys are commonly used due to their optimal combination of physical, chemical, and mechanical properties [2]. The main advantage of titanium is its exceptional biocompatibility with living tissues, corrosion resistance in human environments, and non-toxicity [3]. However, the high modulus of elasticity (approximately 110 GPa) [4, 5] of titanium can lead to the shielding of bone tissue from mechanical loads and to its subsequent degradation.

To increase strength and decrease the modulus of elasticity, stabilizing elements such as Mo, V, Fe, Cr, Nb, etc. are introduced into the titanium alloy [5 – 7]. Titanium alloys with the addition of Nb have been developed for medical use, which have a relatively low modulus of elasticity (about 60 GPa) [8, 9]. The concentration of Nb in medical alloys varies from 15 to 45% [10].

Magnesium and its alloys are classified as bioresorbable materials, which means that they can gradually dissolve within the body's environment and be replaced with natural bone tissue [11,12]. They have low density — 1.74 g/cm^3 for pure Mg [13], moreover, the modulus of elasticity of magnesium is close to that of human bone, at ≈45 GPa [14]. The bioresorbability of magnesium alloys is a favorable characteristic, as it eliminates the need for repeat implant replacement surgeries. However, a limitation in the use of magnesium and its alloys, especially in traumatology and orthopedics, is their rapid corrosion in the physiological environment of the body [15].

Biocoatings are widely used in medicine to reduce the dissolution rate of magnesium alloys and enhance the biological activity of titanium-based implantable devices. A promising approach is to modify the surface of metal

implants by applying coatings using micro-arc oxidation (MAO), otherwise known as plasma electrolytic oxidation (PEO) [16,17]. The synthesis of a coating using the MAO method occurs as a result of numerous micro-arc discharges that migrate along the surface of a metal being treated [18]. This is a complex process that includes diffusion, chemical, plasmochemical, and electrophysical processes involving the substrate material [17–19]. It is known that discharges are formed due to dielectric breakdown of an oxide film when the critical voltage value between the metal substrate and the layer of counterions in the electrolyte at the boundary with the oxide layer is reached [19–21]. In this regard, studies on the identification of the influence of electrophysical characteristics of the transition oxide layer between the metal and the coating on the micro-arc oxidation process, as well as on the formation and properties of micro-arc coatings, are of great interest [22].

The aim of this study was to investigate the patterns of biocoating formation on the surface of titanium alloys and magnesium alloy using the MAO method in electrolytes containing β-tricalcium phosphate particles. The study also aimed to identify the impact of the electrophysical properties of the oxide layer formed during the initial stages of the MAO process on the formation of micro-arc discharges and the properties of the biocoatings formed.

2. Materials and methods

For the study, metal samples were used — plates measuring 10×10×1 mm^3 made of titanium alloys VT1-0 (Ti) (Grade 2) (VSMPO-AVISMA, Verkhnyaya Salda, Russia) and Ti-40 wt.% Nb (Ti-Nb) (Chepetsk Mechanical Plant, Glazov, Russia), as well as Mg-0.8 wt.% Ca (Mg) magnesium alloy (Helmholtz Zentrum Geesthacht, Hamburg, Germany). Before applying the coating using the MAO method, the surface of the samples was treated with P400, P600 and P1000 sanding paper. Further sample preparation included cleaning the samples with ethanol in an ultrasonic washer for 30 minutes and drying in a drying oven for 30 minutes at a temperature of 150°C.

For the formation of coatings using the MAO technique, an electrolyte suspension was prepared containing the following components (in g/L): NaOH — 10, $Na_2HPO_4 \cdot 12H_2O$ — 30, NaF — 5, β-$Ca_3(PO_4)_2$ (β-tricalcium phosphate (β-TCP)) — 60.

To synthesize coatings on metal substrates using the MAO method, a pilot experimental unit "Micro-Arc 3.0" (ISPMS SB RAS, Tomsk, Russia) was used. The MAO process was carried out with the following parameters: pulse duration — 100 μs, pulse frequency — 50 Hz, voltage — 350–500 V, process duration — 5 min.

The morphology of the coating surface was studied using a scanning electron microscope (SEM) (LEO EVO 50, Zeiss, Germany) with an attachment for energy-dispersive X-ray analysis (EDX, INCA, Oxford Instruments, UK) and a transmission electron microscope (JEM-2100, Jeol Ltd., Tokyo, Japan) in "Nanotech" center at ISPMS SB RAS (Tomsk, Russia). The R_a surface roughness was studied on a three-dimensional measuring laser profilometer OLYMPUS OLS5000 (Japan). The pore sizes in the coatings were determined by the secant method from SEM images using the Adobe Photoshop CS3 software package. The structure and phase composition of the coatings were studied by X-ray phase analysis on a DRON-7 diffractometer (IC Burevestnik, Russia) ("Nanotech" center). The survey was carried out in the 2θ angle range of 5–90° with a scanning step of 0.02°, with $Co_{K\alpha}$ radiation (λ = 0.17902 nm). The Joint Committee on Powder Diffraction Standards (JCPDS) database was used to identify phases and interpret the data obtained. The adhesion of the coating to the substrate was assessed using the scratch method on a Revetest RST macro scratch tester (CSM Instruments, USA). The indenter radius and maximum indentation load were 200 μm and 20 N, respectively, and the scratch length was 5 mm. To obtain statistically significant data, each measurement was repeated at least three times for all samples.

3. Results

3.1. Formation of micro-arc CaP coatings on Ti, Ti-Nb and Mg substrates

Based on the graphs of current density versus time, obtained for the MAO coating formation process on various metal substrates at 400 V, two distinct periods can be identified (Fig. 1). During the first 100-second period, there is a significant decrease in current density. This, at a constant voltage, implies an increase in resistance, which is attributed to the active formation of the dielectric coating.

The highest value of the current density at the initial moment of time, equal to 0.68 A/cm^2, is observed for the MAO process during the formation of CaP coatings on Mg substrates. The current densities on Ti and Ti-Nb at the initial time of the process have lower values than on the magnesium substrate, at 0.5 and 0.58 A/cm^2, respectively. In the second period of the process, the current density does not change and at the final moment has a value in the range from 0.04 to 0.11 A/cm^2, depending on the type of substrate.

The difference in the initial current density values for the three substrates can be attributed to the different electrophysical properties of both the substrate material itself and the thin barrier oxide layer formed during the first seconds of the MAO process [23].

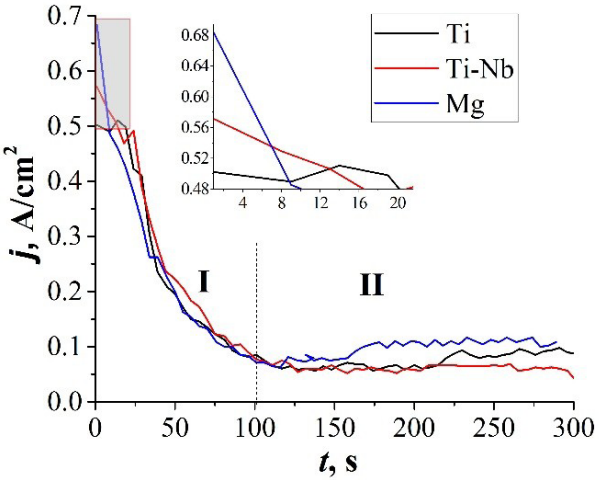

Fig. 1. (Color online) Dependences of current density on the duration of the MAO process at process voltages of 400 V.

3.2. Analysis of the pore structure of CaP coatings on Ti, Ti-Nb, and Mg substrates

A significant aspect of the MAO process is that the sequence of discharges tends to repeat in specific areas of the sample surface, occurring in the form of "cascades" that typically consist of hundreds or even thousands of individual discharges [19]. It has been determined that the presence of deep pores created through the sparking of these discharges determines the location of the subsequent sequence of discharges, forming an area with relatively low electrical resistance [19, 20].

Analysis of cross-sectional micrographs of CaP-coated samples with different substrate types (Fig. 2) reveals that the coatings exhibit a porous structure. The coating deposited on the Ti substrate displays pores and cavities with varying geometries and sizes (Fig. 2 a), which may suggest a different sparking mechanism for micro-discharges. Additionally, there are small pores that are organized in elongated groups in specific directions.

The CaP coatings on the Ti-Nb alloy (Fig. 2 b) exhibit a denser structure. There are large accumulations of small pores (less than 1 μm) observed on the surface of the coating. The presence of these groups of small pores suggests the formation of low-intensity discharge cascades.

For the coatings on Mg, it can be observed that the boundary at the metal-coating interface has an uneven character (Fig. 2 c). During the synthesis of CaP coatings on an Mg substrate by the MAO method, the coating formation front begins to actively move deeper into the substrate. The higher the voltage of the MAO process, the higher the local temperatures develop in the area of micro-arc discharge channels, leading to an intensification of the process of coating embedding into the substrate and deeper areas of embedding.

The surface of coatings on all types of substrates (Ti, Ti-Nb and Mg) is also porous (Fig. 3 a – c). In addition, dispersed β-TCP particles are present on the surface of the coatings, which precipitate from the electrolyte. Due to high temperatures, β-TCP particles melt in the micro-arc discharge channel. However, at the final stage of the process, when the current density becomes minimal, the dispersed particles from the electrolyte are transferred to the surface of the coating, which has not yet fully solidified, and, once there, remain morphologically unchanged, partially fused into the surface (Fig. 3 a – c).

An analysis of the pore structure in SEM images of the coatings (Fig. 3 a – c) reveals that on the surfaces of CaP coatings deposited on Ti and Ti-Nb substrates, large pores measuring 5 – 7 μm are present, indicating intense micro-arc discharges. Additionally, groups of smaller pores measuring less than 1 μm are observed, which are the result of less intense cascades of micro-arc discharges (indicated by arrows). A distinctive feature of the coatings deposited on Mg substrates is that a paucity of small pores were detected, mainly large pores with a diameter of up to 10 μm were present. These larger pores are likely a result of more powerful micro-arc discharges occurring during the coating process.

Figure 3 d – f shows histograms of the pore size distribution on the surface of CaP coatings synthesized on various substrates at a voltage of 400 V after 1, 3 and 5 minutes of the MAO process. It was found that with the increasing duration of the MAO process, the pore sizes increase, in coatings on Ti-substrates — up to 8 μm, and on Ti-Nb and Mg-substrates — up to 13 μm. As the thickness of the dielectric layer increases, the current density decreases and there are fewer discharges on the surface. However, the discharges that do occur become more powerful [24]. It should be noted that Ti and Ti-Nb coatings have a high content of pores between 1 and 2 μm, while coatings deposited on Mg have significantly less of pores up to 1 μm in size.

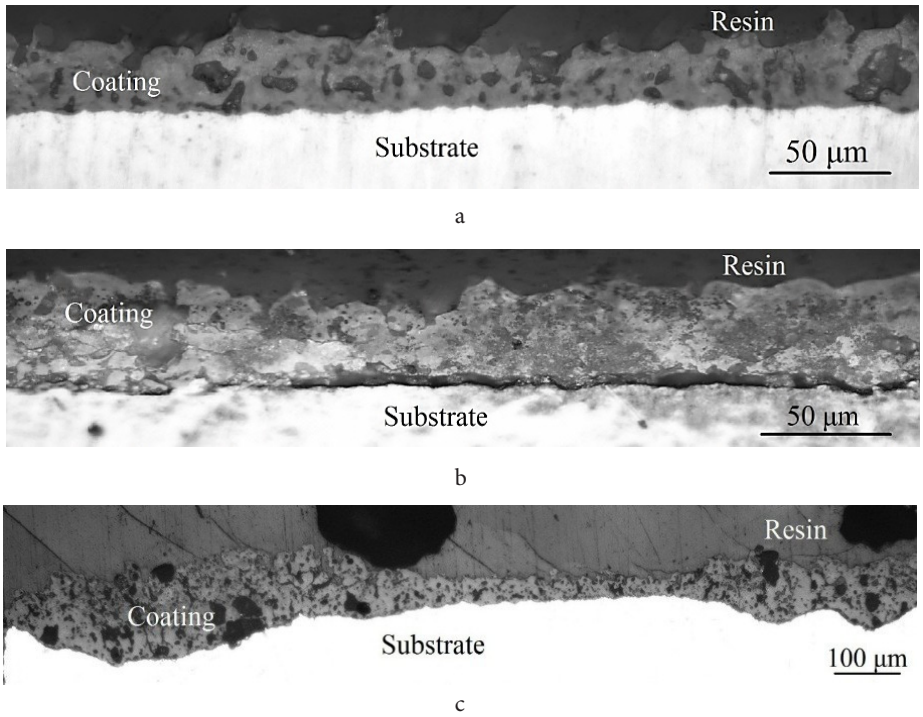

Fig. 2. SEM images of cross-sections of samples with CaP coatings on Ti (a), Ti-Nb (b) and Mg (c) obtained at a process voltage of 400 V.

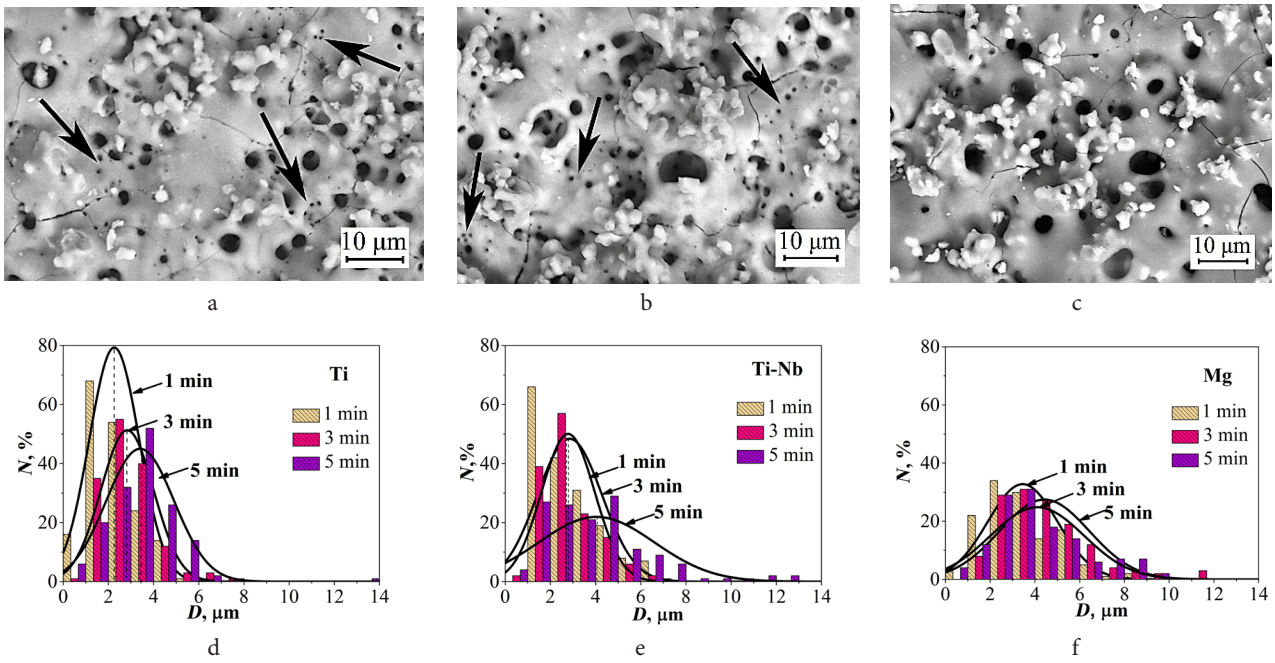

Fig. 3. (Color online) SEM images of the surface of CaP coatings obtained on Ti (a), Ti-Nb (c) and Mg (e) at a voltage of 400 V; histograms of pore size distribution on the surface of CaP coatings on Ti (d), Ti-Nb (e) and Mg (f) after 1, 3, and 5 minutes of application.

3.3. Phase composition and fine structure of CaP coatings on Ti, Ti-Nb, and Mg substrates

Figure S1 in Supplementary materials shows the X-ray diffraction patterns of the coatings obtained on Ti, Ti-Nb, and Mg substrates at different application times of 1, 3, and 5 minutes, respectively. We found that in the CaP coatings, starting from the first minute of the MAO process, all crystalline phases began to form on all types of substrates, including those corresponding to calcium-phosphate compounds. The presence of the following crystalline phases was detected in the coatings: α-TCP (ICDD #09-0348), β-TCP (ICDD #09-0169), and titanium oxide in the form of anatase (A) (ICDD #21-1272). A diffuse scattering region was observed in the 2θ angle range of 10 – 25°, indicating the presence of an amorphous phase. As the processing time increased, the crystallization process in the coatings intensified.

Using transmission electron microscopy, the fine structure and elemental composition of the substrate-coating transition layer were studied on thin sections of metal samples with CaP coatings (Fig. 4). Figure 4 a shows a TEM image of a cross-section of a CaP-coated Ti sample, in which a transition layer of the substrate-coating system is observed. This layer can be divided into two parts: a thin non-porous layer with a thickness of about 50 nm and a porous layer with a thickness of about 350 nm, with pores measuring 100 – 150 nm. The presence of pores indicates the beginning of the MAO process and the appearance of the first spark discharges.

The points are marked in Fig. 4 a (1, 2, 3, 4, 5, 6 and 7), in which the analysis of the elemental composition of the coating was carried out, presented in Table 1. Point 5 is located in the area of a thin non-porous layer dominated by the elements Ti and O, which indicates that this area belongs to the transition oxide layer. In points 3 and 4, in the region of the porous oxide layer, in addition to Ti and O, P and Ca are present in small amounts, which also indicates the initial appearance of micro-arc discharges trapping the electrolyte components. Points 1 and 2 are characterized by a high content of P (23.6 and

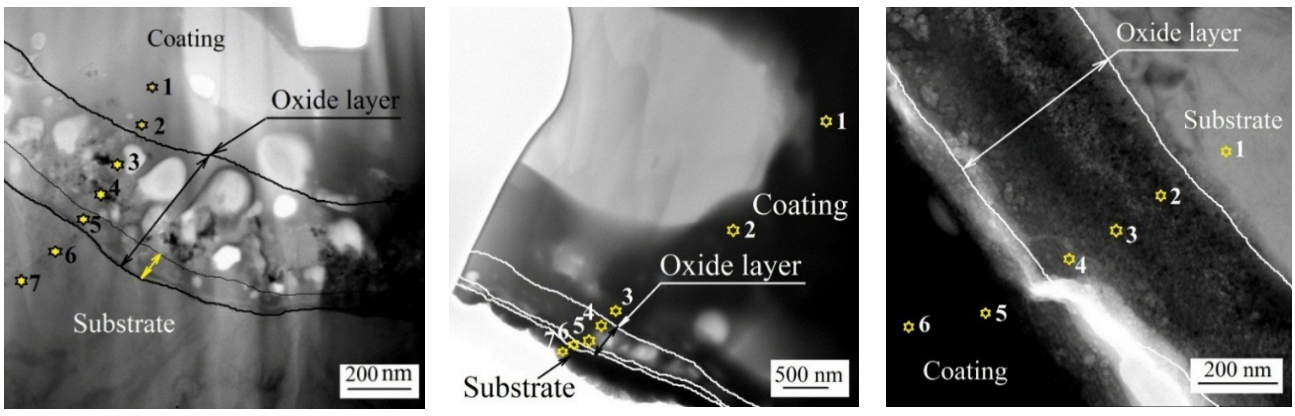

Fig. 4. TEM images of cross-sections of CaP coatings on Ti (b), Ti-Nb (d) and Mg (f) substrates.

Table 1. The elemental composition of CaP coatings on Ti, Ti-Nb and Mg, determined by the EDX method in selected points, at.%.

Substrate	Point	O	P	Ca	Ti	Nb	Mg	F
Ti	1	52.8	23.6	0.3	23.3	–	–	–
	2	47.6	18.5	0.2	33.7	–	–	–
	3	47.0	6.8	0.3	45.9	–	–	–
	4	47.5	6.2	0.3	46.0	–	–	–
	5	46.5	0.5	0.0	53.0	–	–	–
	6	3.4	0.0	0.0	96.6	–	–	–
	7	3.2	0.0	0.0	96.8	–	–	–
Ti-Nb	1	30.5	22.6	1.5	34.7	11.7	–	–
	2	33.5	20.8	1.6	31.5	12.5	–	–
	3	40.4	16.3	1.0	32.4	9.9	–	–
	4	45.7	5.6	0.0	31.4	17.3	–	–
	5	43.2	2.4	0.0	37.0	17.4		
	6	20.3	1.5	0.0	52.3	25.9		
	7	2.5	0.0	0.0	65.2	32.3		
Mg	1	4.3	0.0	0.0	–	–	95.5	0.2
	2	56.4	1.6	0.0	–	–	35.3	6.7
	3	56.3	1.9	0.0	–	–	34.8	7.0
	4	54.4	2.6	0.6	–	–	34.3	8.1
	5	55.2	13.1	0.4	–	–	27.2	4.1
	6	55.9	12.6	1.2	–	–	27.3	3.0

18.5 at.%, respectively). This is the CaP region of the coating, but near the metal substrate this region is characterized by a low Ca content (0.2 – 0.3 at.%). At points 6 and 7, Ti is mainly present, since they are located in the substrate area.

The TEM image of the cross-section of the CaP coating on the Ti-Nb alloy (Fig. 4b) highlights the substrate region (point 7), the transition oxide layer region (points 4, 5, and 6), and the coating region (points 1, 2, and 3). In point 7, the dominant elements are Ti and Nb (Table 1), indicating that the substrate is made of these materials. Points 4, 5, and 6 show the presence of Ti, Nb, and O, indicating the presence of a transition oxide layer, similar to what is found on a Ti substrate. This layer is composed of a non-porous region with a thickness of approximately 50 nm and a porous region with a thickness between 300 and 500 nm. Points 1, 2, and 3 have a high P content (16.3, 20.8, and 22.6 at.%, respectively) and also contain Ca, as they are located within the CaP coating region.

Unlike Ti and Ti-Nb substrates, the transition oxide layer on Mg has a thickness of ≈500 nm (Fig. 4c) and is dense (non-porous). The elemental composition of the transition layer, defined in points 2, 3, 4, is characterized by a predominant content of Mg and O (Table 1). There is also the presence of F in these areas, which was introduced into the electrolyte in the form of NaF [25]. Mg is predominantly present in the elemental composition of point 1, located in the substrate region, and P and Ca appear in the compositions of points 5 and 6, since they are located in the CaP region of the coating.

3.4. Structural and mechanical properties of CaP coatings

Many studies have noted a significant effect of the voltage of the MAO process on the structural, mechanical and morphological properties of coatings [26, 27]. These patterns were also identified in the presented work. With an increase in voltage from 350 to 500 V during the MAO process, the thickness (d, μm) of CaP coatings increased linearly on all types of substrates: from 27 to 81 μm on Ti, from 46 to 70 μm on Ti-Nb, and from 83 to 118 μm on Mg (Fig. 5a).

An increase in voltage also contributes to an increase in the roughness values (R_a, μm) of CaP coatings (Fig. 5b): from 2 to 4 μm on Ti, from 4 to 7.8 μm on Ti-Nb, and from 5.5 to 8.8 μm on Mg. Thus, the graphs of changes in roughness correlate with the graphs of changes in the thickness of CaP coatings — as the thickness of the coatings increases, the roughness also increases.

It should be noted that thickness and roughness have the maximum value for coatings on Mg substrate. Evidently, this is also a consequence of the more intense micro-arc discharges that occur on Mg.

The adhesive properties of coatings on different types of substrates were investigated by scratch testing. The quantitative measure of the adhesion strength of the coating in the study by this method is the load exerted by the indenter when scratching the coating, at which the coating completely detaches from the substrate (L_c, N). It was found that for the coatings on Ti, with an increase in the MAO process voltage from 350 to 450 V, the critical load value increases from 10 to 12.3 N, and with a further increase to 500 V, it decreases to the initial value of 10 N (Fig. 5c). A similar pattern is observed for coatings on Ti-Nb. However, in the voltage range of 350 – 450 V, the critical load varies between 8 – 9 N. When the voltage is increased to 500 V, the critical load value decreases to 7 N. The dependence of the change in critical load for the coatings on Mg is fundamentally different from the coatings on titanium alloys. In the voltage

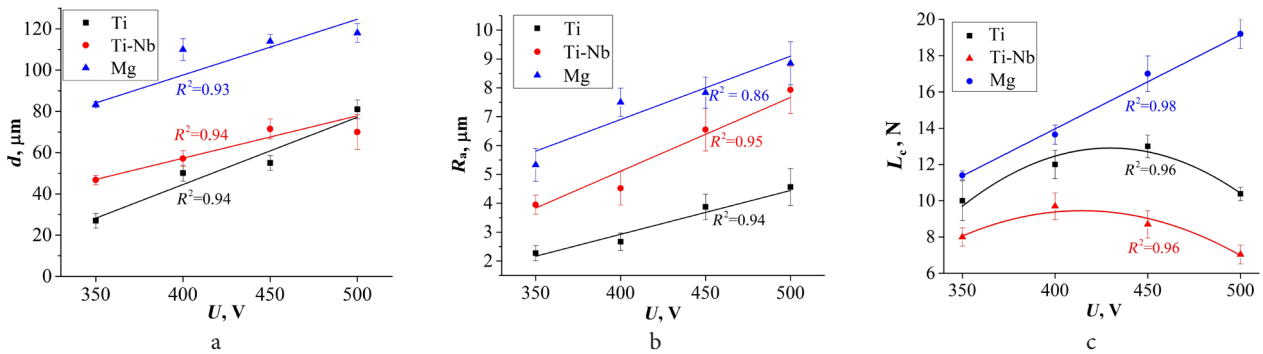

Fig. 5. (Color onlline) Changes in thickness (a), roughness (b), and critical load during scratch testing (c) for CaP coatings on Ti, Ti-Nb, and Mg substrates, depending on the voltage of the MAO process.

range 350 – 500 V, the critical load value increases linearly from 11.5 to 19.2 N. This difference can be explained by the more intense interaction of the magnesium substrate with the electrolyte during the MAO process, as evidenced by the advance of the boundary of the coating formation front deep into the magnesium substrate (Fig. 2 c). In addition, the thickness of the intermediate oxide layer between the coating and the substrate plays an important role in improving adhesion strength. As it was established, for coatings on an Mg substrate the thickness of the non-porous oxide layer is almost 10 times higher than that for coatings on Ti and Ti-Nb (Fig. 4 c). A higher value of the total coating thickness on Mg also plays a positive role in increasing its adhesion strength.

4. Discussion

The processes of formation of micro-arc discharges directly depend on the electrophysical properties of the metal substrate and the transition oxide layer. Table 1S in Supplementary material presents the characteristics of metals used in the work as substrate materials and their oxides. The analysis of the data shows that Mg has the lowest melting point, the highest thermal conductivity, and the lowest electrical resistance. This suggests that the MAO process on an Mg substrate is the most intensive, which is confirmed by the movement of the coating formation front deep into the Mg substrate.

The electrophysical properties of titanium, niobium, and magnesium oxides are also different. P. Kofstad [30] notes that TiO_2 and Nb_2O_5 oxides, as a rule, differ in their nonstoichiometric compositions, which is manifested in a change in structure — the formation of oxygen deficiency (or excess metal). Clyne et al. [19] wrote that electron mobility can be relatively high in some oxides, especially those with variable stoichiometry and high levels of various defects. This leads to an increase in the number of quasi-free electrons, as a result of which these oxides acquire electronic conductivity. For this reason, these oxides are called n-type semiconductors. Thus, for instance, in the case of Nb substrates, the authors [28] state that during anodizing, niobium oxides with other valences are always present at the boundary between the anode oxide film (Nb_2O_5) and the metal substrate (Nb) in the form of transition layers or individual inclusions. The following reaction may occur:

$$Nb + 2Nb_2O_5 = 5NbO_2 \quad (1)$$

Niobium oxides with the lowest degree of oxidation are known to have the most pronounced electrical conductivity in the $Nb_2O_5 – NbO_2 – NbO$ direction [30]. In MgO, deviations from stoichiometry are very insignificant. Cationic vacancies are the main types of defects in MgO. This oxide is therefore characterized by ionic conductivity and can be conditionally classified as a p-type semiconductor (Table 1S).

The breakdown of the oxide layer during a micro-arc discharge can be of different intensity and occur at different levels of accumulated electrical energy. The formation of low-intensity discharge cascades through TiO_2 and Nb_2O_5 oxide layers may be a consequence of the high electrical conductivity of the oxide layer due to the nonstoichiometry of the oxides and the presence of defects in their crystal structure [30, 28]. The authors of [19, 20, 31] also believe that the low value of the band gap, which is characteristic of TiO_2 and Nb_2O_5 oxides, plays an important role in this case (Table S1). In addition, another electrical property has potential significance here, namely the dielectric constant (relative permittivity), which characterizes the ability of a crystal lattice to accumulate an electric charge. It depends on the nature of the bond (the degree of ionization) and the location of the ions [19]. Titanium and niobium oxides have a high dielectric constant and can allow low-intensity micro-arc discharges to pass through (Fig. S2 a).

Magnesium oxide MgO has the largest band gap (Table S1). It is more difficult for electrons in MgO to move from the valence band to the conduction band due to the formation of a high energy barrier, compared with TiO_2 or Nb_2O_5. Only when the electrons accumulate in a higher concentration can they move into the conduction band. As a result, they contribute to the formation of singular intense micro-arc discharges (Fig. S2 b). Magnesium oxide is also characterized by a low value of dielectric constant, a layer of magnesium oxide accumulates a greater amount of electrical energy, which is released in the form of single high-intensity micro-arc discharges.

5. Conclusions

The patterns of formation of CaP coatings by the MAO method on metal substrates of various types were studied: bioinert titanium alloys Ti, Ti-Nb and bioresorbable magnesium alloy Mg. The initial values of the current density for the MAO process on Ti, Ti-Nb, and Mg substrates were 0.5, 0.58, and 0.68 A/cm^2, respectively. The thickness of the non-porous oxide layer for coatings on Ti and Ti-Nb substrates was 50 nm, and on the Mg substrate it was approximately 500 nm. In addition to large pores up to 5 – 7 μm in size, groups of small pores less than 1 μm in size were present on the surfaces of Ti and Ti-Nb coatings, indicating cascades of low-intensity micro-arc discharges. Whereas on the surface of coatings on Mg substrates, large individual pores of 10 μm were observed, indicating intense micro-arc charges.

The maximum coating thicknesses on Ti and Ti-Nb were 81 μm and 70 μm, and the R_a roughness values were 4.0 μm and 7.8 μm, respectively. For coatings on Mg substrates, these values were higher and amounted to 118 μm and 8.8 μm, respectively. The maximum critical load values for Ti, Ti-Nb, and Mg coatings were 12.3, 9.0, and 19.2 N, respectively. Thus, due to the more intensive MAO processes, coatings on Mg alloy are superior in their structural and mechanical properties to coatings on titanium alloys.

TiO_2, Nb_2O_5, and MgO oxides have different types of conductivity, band gap, and dielectric constant, which affects the intensity and nature of sparking of the discharges that occur during the MAO process. Evidently this is the main reason for the different properties of the coatings formed on Ti, Ti-Nb and Mg substrates.

Supplementary material: *The online version of this paper contains supplementary material freely available at the journal's web site https://lettersonmaterials.com.*

References

1. M. Alonzo, F.A. Primo, S.A. Kumar, J.A. Mudloff, E. Dominguez, G. Fregoso, N. Ortiz, W.M. Weiss, B. Joddar, Bone tissue engineering techniques, advances, and scaffolds for treatment of bone defects, Current Opinion in Biomedical Engineering 17 (2021) 100248.
2. A. Festas, A. Ramos, J.P. Davim, Machining of titanium alloys for medical application — a review, Proc. Inst. Mech. Eng. B. J. Eng. Manufac. 236 (4) (2022) 309–318.
3. L.C. Zhang, L.Y. Chen, L.Q. Wang, Surface modification of titanium and titanium alloys: technologies, developments, and future interests. Adv. Eng. Mater. 22 (5) (2019) 1901258.
4. J. Xu, J. Zhang, Y. Shi, J. Tang, D. Huang, M. Yan, M. Dargusch, Surface modification of biomedical Ti and Ti alloys: A Review on current advances, Materials 15 (2022) 1749.
5. M. Niinomi, Mechanical properties of biomedical titanium alloys, Mater. Sci. Eng. 243 (1998) 231–236.
6. N. Koju, S. Niraula, B. Fotovvati, Additively manufactured porous Ti6Al4V for bone implants: A Review, Metals 12 (4) (2022) 687.
7. M.P. Nikolova, M.D. Apostolova, Advances in multifunctional bioactive coatings for metallic bone implants, Materials 16 (1) (2022) 183.
8. K. Zhuravleva, S. Scudino, M.S. Khoshkhoo, A. Gebert, Mechanical alloying of β-type Ti-Nb for biomedical applications, Adv. Eng. Mater. 15 (4) (2013) 262–268.
9. K. Zhuravleva, M. Bönisch, S. Scudino, M. Calin, Phase transformations in ball-milled Ti-40Nb and Ti-45Nb powders upon quenching from the β-phase region, Powder Technology 253 (2014) 166–171.
10. K. Zhuravleva, R. Müller, L. Schultz, Determination of the Young's modulus of porous β-type Ti-40Nb by finite element analysis, Mater. Des. 64 (2014) 1–8.
11. V. Tsakiris, C. Tardei, F.M. Clicinschi, Biodegradable Mg alloys for orthopedic implants — A review, J. Magnes. Alloy. 9 (2021) 1884–1905.
12. R.B. Heimann, Magnesium alloys for biomedical application: Advanced corrosion control through surface coating, Surf. Coat. Technol. 405 (2021) 126521.
13. Y. Li, H. Jahr, J. Zhou, A.A. Zadpoor, Additively manufactured biodegradable porous metals, Acta Biomater. 115 (2020) 29–50.
14. X. Guo, Y. Hu, K. Yuan, Y. Qiao, Review of the effect of surface coating modification on magnesium alloy biocompatibility, Materials 15 (2022) 3291.
15. M.B. Sedelnikova, A.V. Ugodchikova, T.V. Tolkacheva, V.V. Chebodaeva, I.A. Gluklhov, M.A. Khimich, O.V. Bakina, M.I. Lerner, V.S. Egorkin, J. Schmidt, Yu. P. Sharkeev, Surface modification of Mg0.8Ca alloy via wollastonite micro-arc coatings: significant improvement in corrosion resistance, Metals 11 (2021) 754.
16. G.B. Darband, M. Aliofkhazraei, P. Hamghalam, N. Valizade, Plasma electrolytic oxidation of magnesium and its alloys: Mechanism, properties and applications, J. Magnes. Alloy. 5 (2017) 74–132.
17. D. Wang, X. Liu, Y. Wang, Q. Zhang, D. Li, X. Liu, H. Su, Y. Zhang, S. Yu, D. Shen, Role of the electrolyte composition in establishing plasma discharges and coating growth process during a micro-arc oxidation, Surf. Coat. Technol. 402 (2020) 126349.
18. M. Aliofkhazraei, D.D. Macdonald, E. Matykina, V.S. Egorkin, E.V. Parfenov, J.A. Curran, S.C. Troughton, S.L. Sinebryukhov, S.V. Gnedenkov, T. Lampke, F. Simchen, H.F. Nabavi, Review of plasma electrolytic oxidation of titanium substrates: Mechanism, properties, applications and limitations, Appl. Surf. Sci. Adv. 5 (2021) 100121.
19. T.W. Clyne, S.C. Troughton, A review of recent work on discharge characteristics during plasma electrolytic oxidation of various metals, Int. Mater. Rev. 64 (3) (2019) 127–162.
20. A. Nominé, S.C. Troughton, A.V. Nominé, G. Henrion, T.W. Clyne, High speed video evidence for localised discharge cascades during plasma electrolytic oxidation, Sur. Coat. Technol. 269 (2015) 125–130.
21. F. Simchen, M. Sieber, A. Kopp, T. Lampke, Introduction to plasma electrolytic oxidation — An overview of the process and applications, Coatings 10 (7) (2020) 628.
22. M.B. Sedelnikova, A.V. Ugodchikova, P.V. Uvarkin, Yu.P. Sharkeev, M.A. Khimich, T.V. Tolkacheva, V.V. Chebodaeva, I.A. Khlusov, Yu. Schmidt, Influence of the substrate material on the formation and properties of micro-arc coatings with particles of β-tricalcium phosphate, Russian Physics Journal 65 (6) (2022) 1048–1057.
23. E.V. Legostaeva, K.S. Kulyashova, E.G. Komarova, M. Epple, Yu. P. Sharkeev, I.A. Khlusov, Physical, chemical and biological properties of micro-arc deposited calcium phosphate coatings on titanium and zirconium-niobium alloy, Materialwissenschaft und Werkstofftechnik 44 (2013) 188–197.
24. S. Sikdar, P.V. Menezes, R. Maccione, T. Jacob, P.L. Menezes, Plasma electrolytic oxidation (PEO) process — processing, properties, and applications, Nanomaterials 11 (6) (2021) 1375.
25. N. Singh, U. Batra, K. Kumar, N. Ahuja, A. Mahapatro, Progress in bioactive surface coatings on biodegradable Mg alloys: A critical review towards clinical translation, Bioactive Materials 19 (2023) 717–757.
26. M.B. Sedelnikova, V.V. Mayer, O.V. Bakina, A.D. Kashin, P.V. Uvarkin, M.A. Khimich, N.A. Luginin, I.A. Glukhov, T.V. Tolkacheva, A.V. Ugodchikova, Y.P. Sharkeev, Antibacterial amorphous-crystalline coatings based on wollastonite and ZnO particles, Crystals 14 (2024) 886.
27. E.G. Komarova, Y.P. Sharkeev, M.B. Sedelnikova, K.A. Prosolov, I.A. Khlusov, O. Prymak, M. Epple, Zn- or Cu-containing CaP-based coatings formed by micro-arc oxidation on titanium and Ti-40Nb alloy: Part I — microstructure, composition and properties. Materials 13 (2020) 4116.
28. H. Shimizu, H. Sato, S. Nishimura, M. Honda, Electrical properties of anodically oxidized Nb_2O_5 and Si-doped Nb_2O_5 films, Jpn. J. Appl. Phys. 44 (2005) 6664.
29. J. Robertson, High dielectric constant gate oxides for metal oxide Si transistors, Rep. Prog. Phys. 69 (2006) 327–396.
30. P. Kofstad, Nonstoichiometry, diffusion and electrical conductivity in binary metal oxides, Wiley — Interscience, New York, 1972, 396 p.
31. S.C. Troughton, A. Nominé, J. Dean, T.W. Clyne, Effect of individual discharge cascades on the microstructure of plasma electrolytic oxidation coatings, App. Surf. Sci. 389 (2016) 260–269.